Photonuclear reactions on ^{59}Co at bremsstrahlung end-point energies of 40–130 MeV*

F. A. Rasulova[1,2†] S. S. Belyshev[3,4] M. A. Demichev[1] D. L. Demin[1] S. A. Evseev[1] N. Yu. Fursova[3,4] M. I. Gostkin[1] J. H. Khushvaktov[1,2] V. V. Kobets[1] A. A. Kuznetsov[3,4] S. V. Rozov[1] E. T. Ruziev[2] A. A. Solnyshkin[1] T. N. Tran[1,5] E. A. Yakushev[1] B. S. Yuldashev[1,2]

[1]Joint Institute for Nuclear Research, Dubna, Russia
[2]Institute of Nuclear Physics of the Academy of Sciences of the Republic of Uzbekistan, Tashkent, Uzbekistan
[3]Skobeltsyn Institute of Nuclear Physics of Lomonosov Moscow State University, Moscow, Russia
[4]Faculty of Physics of Lomonosov Moscow State University, Moscow, Russia
[5]Institute of physics, Vietnam Academy of Science and Technology, Hanoi, Vietnam

Abstract: Relative yields were measured in the 40−130 MeV bremsstrahlung induced reactions of ^{59}Co. The experiments were performed with the beam from the electron linear accelerator LINAC-200 using the activation and off-line γ-ray spectrometric techniques. The bremsstrahlung photon flux was calculated with the Geant4 program. The cross sections were calculated by using the computer code TALYS-1.96 with different models and were found to be in good agreement with the experimental data.

Keywords: photonuclear reaction, relative yields, giant dipole resonance, TALYS, Geant4

DOI: 10.1088/1674-1137/ad6d41

I. INTRODUCTION

The photon-induced reaction cross sections of ^{59}Co are important for designing conventional reactors, fast reactors, and accelerator-driven systems (ADSs). The high-energy photon-induced reactions of ^{59}Co can be used for production of important medical isotopes, such as ^{55}Co, ^{56}Co, ^{57}Co, and ^{58}Co, owing to their suitable decay characteristics. Moreover, ^{59}Co is often used as a monitor target during the study of photonuclear reactions to determine the photon of gamma rays or the accelerator current.

The ^{59}Co(γ, xn)$^{58\text{-}56}$Co reaction cross sections already covered in Refs. [1–5] are only for monoenergetic photons in the energy range from 9.65 to 36.504 MeV. The flux-averaged cross-sections for the ^{59}Co(γ, xn)$^{58\text{-}55}$Co reaction were measured using the method of activation at the bremsstrahlung end-point energies of 15 MeV [6], 22 MeV [7], 25 MeV [8], 30 MeV [9], 65, and 75 MeV [10]. In Ref. [11], the yields of the reactions (γ, 2n), (γ, 3n), (γ, 4n), and ^{59}Co(γ, 1n2p)^{56}Mn, relative to the yield of the reaction (γ, n), were determined using the measurements of gamma-ray activities induced when irradiating ^{59}Co with the 35- and 54-MeV bremsstrahlung. In Ref. [12], the ^{59}Co(γ, 1n2p)^{56}Mn reaction was investigated in the energy range of 30–260 MeV, and differential effective cross sections were calculated from yield curves using the photon difference method. In Refs. [13, 14], data for photospallation yields were presented in units of mb per equivalent photon from a ^{59}Co target measured at the bremsstrahlung end-point energies of 30 to 1050 MeV.

The present study aimed at obtaining new nuclear data for bremsstrahlung-induced photonuclear reactions on ^{59}Co in the energy range of 40–130 MeV and comparing these data with data reported in the literature [7–10] and theoretical values computed with the program package TALYS1.96 [15].

II. MATERIALS AND METHODS

The experiment was carried out with electron beams at energies in the range of 40–130 MeV. A tungsten plate with a size of 4.5 × 4.5 cm and a thickness of 0.5 cm was used as a converter. In the experiments (E_e = 60, 80, 105, and 130 MeV), cobalt metal samples were irradiated with a bremsstrahlung flux formed in the tungsten converter. To compare the results of experiments performed under different conditions at an energy of 40 MeV, the target was directly irradiated with the electron beam. The main parameters of the experiments are given in Table 1.

Received 21 March 2024; Accepted 8 August 2024; Published online 9 August 2024

* Supported in part by the Ministry of Science and Higher Education of the Russian Federation (075-15-2021-1360), and by the project of the National Center for Physics and Mathematics (NCPM) No. 6 "Nuclear and Radiation Physics," direction 6.5.1

† E-mail: rasulova@jinr.ru

Table 1. Main parameters of the experiments.

	Experiment 1	Experiment 2	Experiment 3	Experiment 4	Experiment 5
Energy of electrons/MeV	40	60	80	105	130
Electron beam pulse current/mA	48	40	40	58	50
Irradiation time/min	20	25	15	20	15.5
Integral number of electrons incident on the tungsten converter, $\times 10^{15}$	7.2 ± 0.72	7.5 ± 0.75	4.5 ± 0.45	8.7 ± 0.87	5.8 ± 0.58
Mass of cobalt target/mg	312.0	155.7	145.8	729.5	372.8
Dimensions of cobalt target, cm×cm	1.25×1.25	1.35×0.6	1.25×0.68	1.25×1.25	1.25×1.25
Cooling time/min	50	56	56	39	107
Measuring time of spectra/day	21.8	12.4	8.2	8.1	28.8

The electron linac was operated in the stable mode with a beam pulse width of 2 μs and a repetition rate of 10 Hz. The electron current was measured with a high-sensitivity inductive current sensor [16]. After irradiation, the target was transferred to the test room, where the induced activity in the irradiated target was measured using a high-purity germanium detector (HPGe detector). The spectra of γ-quanta of irradiated targets in the energy range from 50 keV to 3.7 MeV were measured using a CANBERRA GC3018 HPGe detector with a volume of 145 cm^3. We used the HPGe γ-detector with resolutions of 0.8 keV at 122 keV and of 1.76 keV at 1332 keV in combination with standard measurement electronics and a 8K ADC/MCA (Multiport II Multichannel Analyzer). The relative efficiency of this detector is 34.7%. For γ-activity measurements, the activated sample were placed at 56 and 130 mm from the detector surface to maintain the detector dead time at approximately 5% and reduce counting losses due to the coincidence summing effect. Compton background was missed at approximately 3 hours after irradiation, so the targets were located 10 mm from the detector surface for measuring γ-rays of long-lived isotopes in the target.

Energy and efficiency calibrations of the HPGe detector were carried out using the standard gamma-ray sources ^{22}Na, ^{54}Mn, ^{57}Co, ^{65}Zn, ^{88}Y, ^{113}Sn, ^{133}Ba, ^{139}Ce, ^{152}Eu, ^{207}Bi, and ^{241}Am. The gamma-ray spectra were processed using the program DEIMOS32 [17], which fits the count area of the full-energy peaks with a Gaussian function. The processed peaks were identified on the basis of gamma-ray energy and intensity and the half-life of generated residual nuclei. Typical γ-ray spectra of reaction products from irradiated cobalt with a bremsstrahlung end-point energy of 130 MeV are shown in Fig. 1.

The experimental yields of the reactions $Y_{\rm exp}$ were normalized to one electron of the accelerated beam incident on the bremsstrahlung target and calculated using the following formula:

$$Y_{\rm exp} = \frac{S_p \cdot C_{\rm abs}}{\epsilon \cdot I_\gamma} \frac{t_{\rm real}}{t_{\rm live}} \frac{1}{N} \frac{1}{N_e} \frac{{\rm e}^{\lambda \cdot t_{\rm cool}}}{(1-{\rm e}^{-\lambda \cdot t_{\rm real}})} \frac{\lambda \cdot t_{\rm irr}}{(1-{\rm e}^{-\lambda \cdot t_{\rm irr}})}, \quad (1)$$

where S_p is the full-energy-peak area; ϵ is the full-energy-peak detector efficiency; I_γ is the gamma emission probability; $C_{\rm abs}$ is the correction for self-absorption of gamma rays in the sample; $t_{\rm real}$ and $t_{\rm live}$ are the real and live times of the measurement, respectively; N is the number of atoms in the activation sample; N_e is the integral number of incident electrons; λ is the decay constant; $t_{\rm cool}$ is the cooling time; and $t_{\rm irr}$ is the irradiation time. The main γ-ray energies and intensities used to determine the yield of reaction products are listed in Table 2. The nuclear data in Table 2 were extracted from Ref. [18].

The yields $Y_{\rm theor}$ of photonuclear reactions representing the convolution of the photonuclear reaction cross section $\sigma(E)$ and distribution density of the number of bremsstrahlung photons over energy per one electron of the accelerator $W(E, E_{\gamma{\rm max}})$ were determined as a result of the experiment. For the yield measurement of a natural mixture of isotopes, the result is the yield of isotope production in all possible reactions on the natural mixture:

$$Y_{\rm theor} = \int_{E_{\rm th}}^{E_{\gamma{\rm max}}} \sigma(E)\, W\left(E, E_{\gamma{\rm max}}\right) {\rm d}E, \quad (2)$$

where $E_{\gamma{\rm max}}$ is the kinetic energy of electrons hitting the tungsten radiator, E is the energy of bremsstrahlung photons produced on the radiator, and $E_{\rm th}$ is the threshold of the studied photonuclear reaction.

The use of the relative yields makes it possible to obtain the dependence of the probability of photonuclear reactions on the maximum energy of bremsstrahlung under different experimental conditions. The calibration with respect to the yield of the most probable reaction excludes the influence of the total photon absorption cross section. In our case, the ^{59}Co(γ, n)$^{58m+g}$Co reaction was chosen as a dominant reaction because of its wide application in this capacity. The half-lives of the isotopes ^{58m}Co and ^{58g}Co are 9.10 hours and 70.86 days, respectively. ^{58m}Co decays by IT with a branching fraction of 100%. Given that ^{58m}Co has the single gamma line with E_γ =

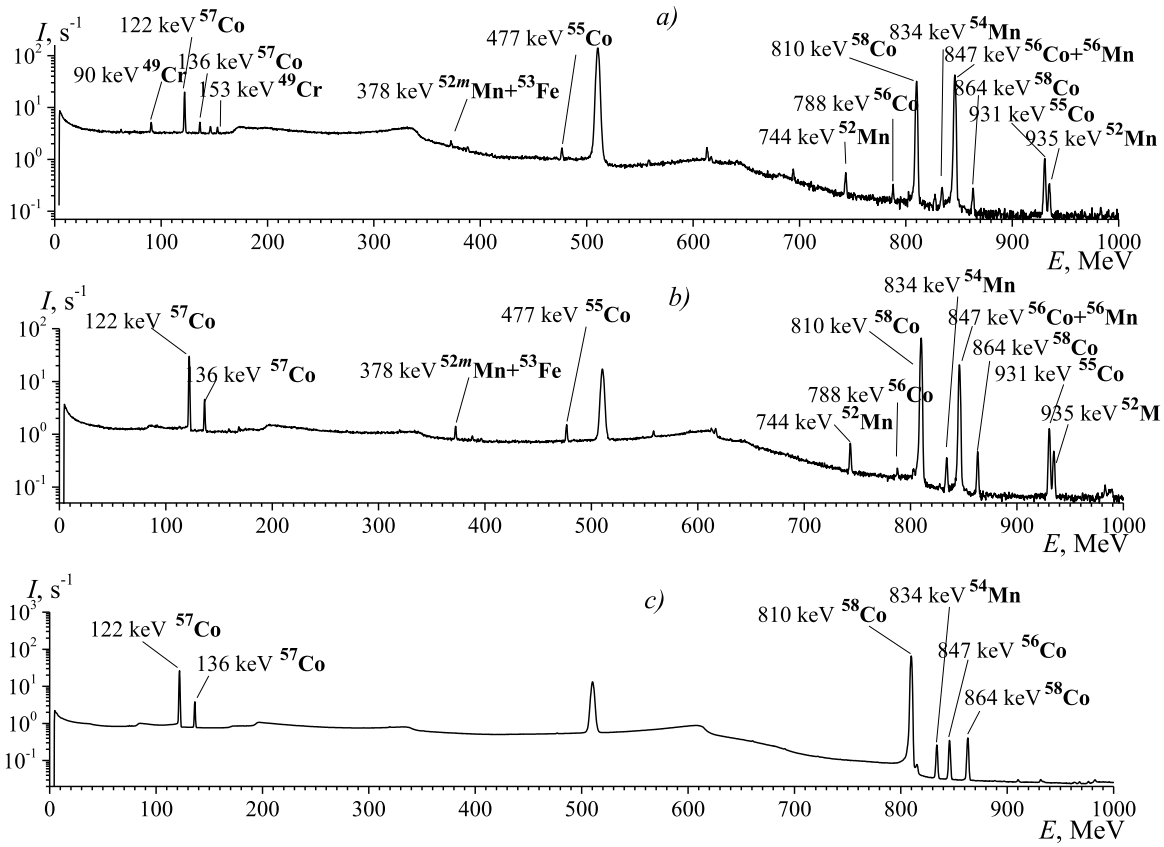

Fig. 1. Spectra of residual activity of the irradiated sample of ^{59}Co (top-to-bottom) at 2 h (a), 6 h (b), and 40 days (c) after irradiation. The spectra measurement duration was 10 min (a), 1 h (b), and 7 days (c), respectively. The bremsstrahlung end-point energy used for the irradiation was 130 MeV.

Table 2. Spectroscopic data from Ref. [18] for product-nuclei from photonuclear reactions.

Product of reaction	Half-life	Reaction	Threshold/MeV	E_γ/keV (I_γ(%))
^{58g}Co	70.86 d	^{59}Co(γ, n)	10.45	810.76 (99.45)
^{58m}Co	9.10 h	^{59}Co(γ, n)	10.48	24.89 (0.0397)
^{57}Co	271.74 d	^{59}Co(γ, 2n)	19.03	122.06 (85.6), 136.47 (10.68)
^{56}Co	77.236 d	^{59}Co(γ, 3n)	30.40	846.77 (99.94), 1037.84 (14.05), 1238.29 (66.46), 1771.36 (15.41), 2598.5 (16.97)
^{55}Co	17.53 h	^{59}Co(γ, 4n)	40.49	477.2 (20.2), 931.1 (75), 1408.5 (16.9)
^{53}Fe	8.51 m	^{59}Co(γ, 5n1p)	58.93	377.88 (42)
^{52}Fe	8.275 h	^{59}Co(γ, 6n1p)	69.61	168.688 (99.2)
^{56}Mn	2.58 h	^{59}Co(γ, 1n2p)	27.98	846.76 (98.85), 1810.73 (26.9), 2113.09 (14.2)
^{54}Mn	312.2 d	^{59}Co(γ, 1n1α)	17.17	834.85 (99.98)
		^{59}Co(γ, 3n2p)	45.46	
^{52g}Mn	5.59 d	^{59}Co(γ, 3n1α)	38.16	744.23 (90), 935.54 (94.5), 1434.06 (100)
		^{59}Co(γ, 5n2p)	66.45	
^{52m}Mn	21.1 min	^{59}Co(γ, 3n1α)	38.54	377.74 (1.68), 1434.06 (98.2)
		^{59}Co(γ, 5n2p)	66.83	
^{51}Cr	27.7 d	^{59}Co(γ, 3n1p1α)	44.71	320.08 (9.91)
		^{59}Co(γ, 5n3p)	73.00	
^{49}Cr	42.3 min	^{59}Co(γ, 5n1p1α)	66.97	62.29 (16.4), 90.64 (53.2), 152.93 (30.3)
		^{59}Co(γ, 7n3p)	95.26	

24.89 keV, it is not possible to experimentally determine the yield of this isotope by the usual method from the peak in the residual activity spectrum; the detector used detects γ-quanta starting from 50 keV. We could determine only the cumulative yield of $^{58m+g}$Co. Thus, the net photopeak counts of ^{58g}Co from different spectra were taken after the decay of more than ten half-lives of ^{58m}Co.

Theoretical values of the relative yields can be calculated using the following formula:

$$Y_{\mathrm{rel},i} = \frac{\int_{E_{\mathrm{th}}}^{E_{\gamma\max}} \sigma_i(E)\, W\left(E, E_{\gamma\max}\right) \mathrm{d}E}{\int_{E_{\mathrm{th}}}^{E_{\gamma\max}} \sigma_{(\gamma,n)}(E)\, W\left(E, E_{\gamma\max}\right) \mathrm{d}E}. \tag{3}$$

Owing to the assumption on the unchanged shape of the bremsstrahlung spectrum, the bremsstrahlung photon production cross section $\sigma(E, E_{\gamma\max})$ must be taken as the function $W(E, E_{\gamma\max})$:

$$Y_{\mathrm{rel},i} = \frac{\int_{E_{\mathrm{th}}}^{E_{\gamma\max}} \sigma_i(E)\, \sigma\left(E, E_{\gamma\max}\right) \mathrm{d}E}{\int_{E_{\mathrm{th}}}^{E_{\gamma\max}} \sigma_{(\gamma,n)}(E)\, \sigma\left(E, E_{\gamma\max}\right) \mathrm{d}E}, \tag{4}$$

where $\sigma(E, E_{\gamma\max})$ is calculated based on the Zeltzer-Berger tables [19].

The total and partial cross sections $\sigma(E)$ of the ^{59}Co(γ, xnyp) reaction were computed for monochromatic photons with the TALYS code. The phenomenological models used below are generally parameterized in terms of Lorentzian forms with giant resonance parameters:

- σ_{Xl}: strength of the giant resonance,
- E_{Xl}: energy of the giant resonance,
- Γ_{Xl}: width of the giant resonance.

The photoreaction cross section data were compared to theoretical calculations on the basis of three standard models of the γSF, namely the Kopecky-Uhl generalized Lorentzian model (GLO) [20], Brink-Axel standard Lorentzian model (SLO) [21, 22], and simplified modified Lorentzian model (MLO) [23]. In addition to these phenomenological models (GLO, SLO, and MLO), two microscopic models, namely the Skyrme-Hartree-Fock-Bogoliubov model with QRPA, proposed by Goriely *et al.* (HFB+QRPA) [24], and the Gogny-Hartree-Fock-Bogoliubov model with QRPA, proposed by Goriely *et al.* (GHF+QRPA) [25], were used. This approach is natural, because it involves the use of a single-particle nuclear level scheme, which means that the individual properties of each nucleus are considered.Fig. 2 shows experimental data and results of TALYS models on the cross section of reactions (γ, n), (γ, 2n), (γ, n)+ (γ, np), and (γ, 1n2p) on ^{59}Co.

GLO was suggested to predict the correct behavior of the $E1$ γ-strength functions in the low-energy range by adopting the temperature-dependent width along with the non-zero limiting value as E_γ goes to zero. We used SLO for all multipoles higher than 1. The MLO model was developed to provide an improved estimate of the E1 and M1 PSFs for all nuclei. The HFB+QRPA model is based on the Skyrme force. In this model, some phenomenological corrections are introduced to take into account the damping of the collective motion as well as the deformation effects. The GHF+QRPA model allows for a consistent description of axially symmetric deformations; it phenomenologically includes the impact of multiparticle multihole configuration as a function of their densities.

The photon flux in the sample was simulated using Geant4 [26]. The energy spectrum of bremsstrahlung in the location of cobalt samples is shown in Fig. 3. In the experiments at 60 and 80 MeV, the shape of the electron beam was round, setting a diameter of 5.5 mm. In the experiments at 40, 105, and 130 MeV, the shape of the electron beam was a rectangle with a size of 2 mm × 20 mm.

III. RESULTS AND DISCUSSION

The relative yields Y_{rel} of the photonuclear reactions measured in the bremsstrahlung end-point energy range of 40–130 MeV from the conducted experiment are given in Table 3 and Figs. 4–7.

A. Reactions with neutron emissions

Figure 4 shows relative yields of the ^{59}Co(γ, xn)^{57,56,55}Co reactions. Within the limits of error, our results on relative yields of the ^{59}Co(γ, 2n)^{57}Co reaction in 40 MeV agree well with calculations based on models GLO, SLO and MLO, and with literature data [13]. The experimental points at 60, 67 [13], and 80 MeV are located at lower positions than the calculated data. Our results on the relative yield of the ^{59}Co(γ, 3n)^{56}Co reaction in 40 MeV agree well with calculations based on model SLO. The experimental points at 40 [13], 60, 67 [13], and 80 MeV are located at lower positions than the calculated data. The experimental points on the relative yield of the ^{59}Co(γ, 4n)^{55}Co reaction are also located at lower positions than the calculated data. Given that there are not sufficient experimental points in this area, we cannot draw clear conclusions on the cross sections.

B. Reactions with the emission of one proton and several neutrons

It can be seen from Fig. 5 that the experimentally obtained relative yields for the ^{59}Co(γ, 6n1p)^{52}Fe reaction at

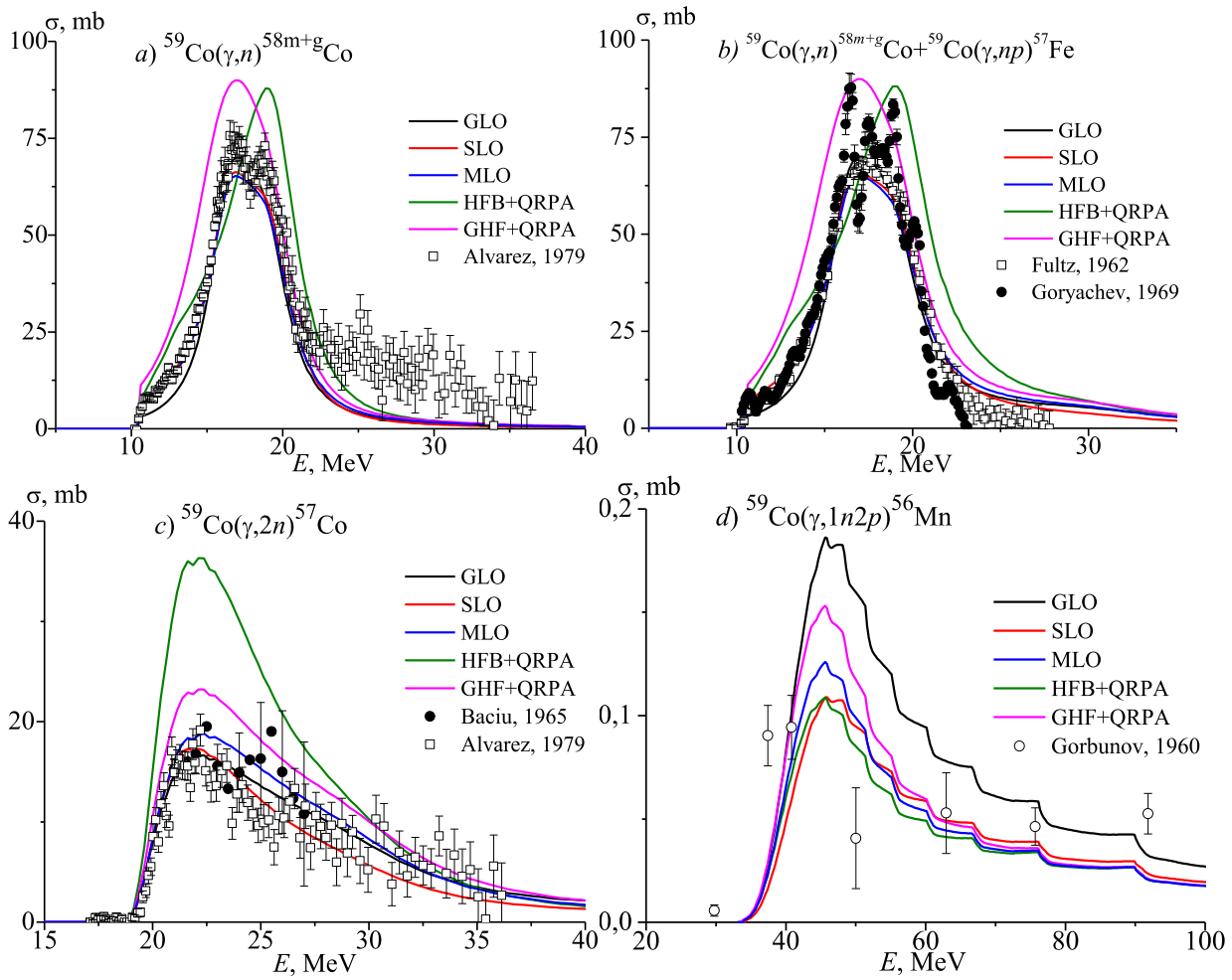

Fig. 2. (color online) Experimental data and results of TALYS models on the cross section of reactions (γ, n) [3], (γ, $2n$) [3, 7], (γ, n)+(γ, np) [4, 9], and (γ, $1n2p$) [12] on ^{59}Co.

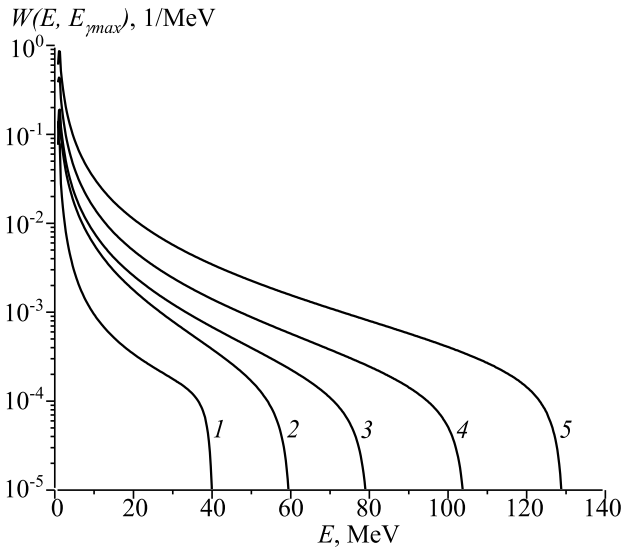

Fig. 3. Distribution density of the number of bremsstrahlung photons at energies of 40 (1), 60 (2), 80 (3), 105 (4), and 130 MeV (5).

energies of 162 and 200 MeV in previous studies [13] are not in agreement with the values simulated with TALYS, according to different models. The experimental points at 130 MeV are in agreement with the calculated values based on different models without GLO.

It can be seen from Fig. 5 that the experimentally obtained relative yields for the ^{59}Co(γ, $5n1p$)^{53}Fe reaction at energy 102 MeV [13] is not in agreement with the values simulated with TALYS, according to different models. The experimental points at 105 MeV are in agreement with the calculated values based on model HFB+QRPA.

C. Reactions with emission of two protons and several neutrons

It can be seen from Fig. 6 that the experimentally obtained relative yields for the production of ^{52g}Mn at the bremsstrahlung end-point energies of 60, 80, and 105 MeV are in agreement with the values simulated with TALYS, according to different models (SLO and MLO). Fig. 6 also shows that the experimentally obtained relat-

Table 3. Relative yields of the photonuclear reactions on ^{59}Co at the bremsstrahlung end-point energies of 40–130 MeV from the conducted experiment.

Isotope	Bremsstrahlung end-point energy/MeV	Relative yields (%)					
		Experiment	TALYS-1.96				
			GLO	SLO	MLO	HFB+QRPA	GHF+QRPA
^{57}Co	40	18 ± 2	23	19	24	29	19
	60	17 ± 2	26	21	26	31	21
	80	17 ± 2	27	22	27	31	21
	105	18 ± 2	28	23	28	32	22
	130	21 ± 2	28	23	28	32	22
^{56}Co	40	0.33 ± 0.04	0.40	0.23	0.34	0.25	0.27
	60	0.32 ± 0.03	1.45	0.81	1.04	0.72	0.84
	80	0.44 ± 0.02	1.82	1.04	1.26	0.87	1.00
	105	0.51 ± 0.04	2.08	1.22	1.43	0.99	1.12
	130	0.52 ± 0.05	2.17	1.34	1.55	1.08	1.20
^{55}Co	60	0.0071 ± 0.0008	0.059	0.033	0.034	0.022	0.026
	80	0.015 ± 0.003	0.125	0.074	0.071	0.047	0.052
	105	0.029 ± 0.005	0.170	0.103	0.098	0.067	0.071
	130	0.091 ± 0.009	0.195	0.125	0.117	0.081	0.084
^{53}Fe	105	0.0056 ± 0.0006	0.048	0.031	0.029	0.021	0.019
^{52}Fe	130	0.0006 ± 0.0001	0.0032	0.0021	0.0019	0.0014	0.0013
^{56}Mn	60	0.048 ± 0.005	0.21	0.11	0.12	0.05	0.06
	80	0.096 ± 0.011	0.43	0.24	0.23	0.11	0.11
	105	0.155 ± 0.016	0.56	0.32	0.31	0.15	0.15
	130	0.396 ± 0.044	0.63	0.38	0.36	0.18	0.17
^{54}Mn	60	0.65 ± 0.07	0.88	0.56	0.81	0.72	0.64
	80	0.77 ± 0.08	1.39	0.87	1.10	0.92	0.85
	105	0.93 ± 0.10	1.85	1.16	1.38	1.13	1.03
	130	1.26 ± 0.14	2.06	1.31	1.52	1.23	1.13
^{52g}Mn	60	0.0044 ± 0.006	0.021	0.012	0.012	0.008	0.009
	80	0.015 ± 0.002	0.064	0.038	0.037	0.025	0.027
	105	0.022 ± 0.003	0.139	0.088	0.084	0.059	0.058
	130	0.137 ± 0.017	0.227	0.149	0.143	0.103	0.098
^{52m}Mn	60	0.0025 ± 0.0005	0.022	0.012	0.012	0.008	0.009
	80	0.019 ± 0.003	0.067	0.039	0.036	0.024	0.026
	105	0.038 ± 0.005	0.138	0.085	0.076	0.054	0.053
	130	0.091 ± 0.012	0.226	0.146	0.130	0.093	0.089
^{51}Cr	105	0.071 ± 0.008	0.24	0.15	0.14	0.10	0.09
	130	0.154 ± 0.014	0.41	0.26	0.24	0.18	0.16
^{49}Cr	105	0.0007 ± 0.0001	0.009	0.006	0.006	0.004	0.004
	130	0.009 ± 0.001	0.031	0.021	0.020	0.014	0.013

ive yields for the production of ^{52m}Mn at the bremsstrahlung end-point energies of 60, 80, and 105 MeV are in agreement with the values simulated with TALYS, according to models SLO and MLO. Literature data [13] are located at much lower positions than the calculated curves.

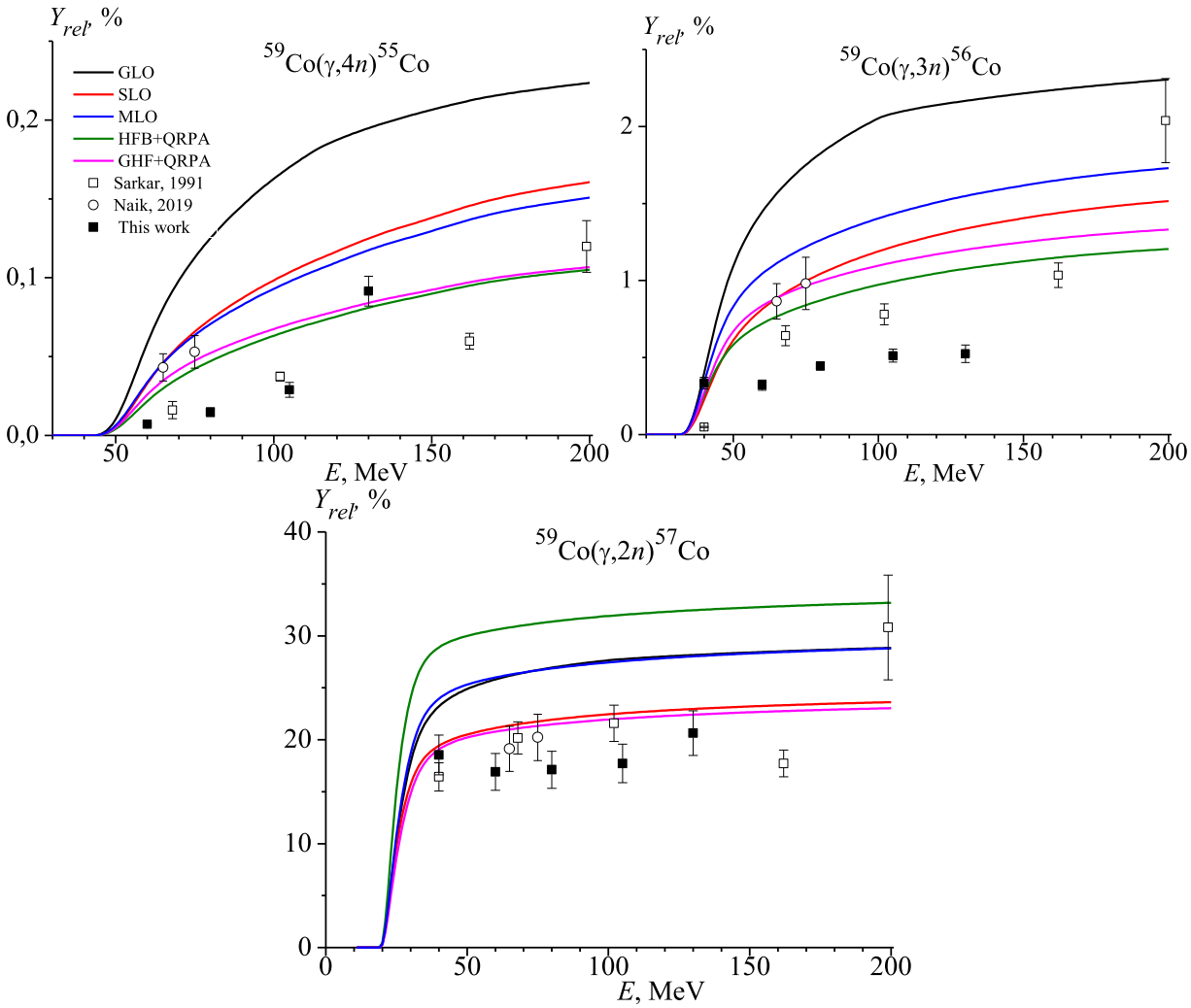

Fig. 4. (color online) Relative yields of the ^{59}Co(γ, xn)^{57,56,55}Co reactions as a function of the bremsstrahlung end-point energy from the present study (solid squares) and literature data, [4] (open triangles), [10] (open circles), and [13] (open squares), as well as theoretically calculated values using different models for the $E1$ gamma-ray strength function in TALYS values.

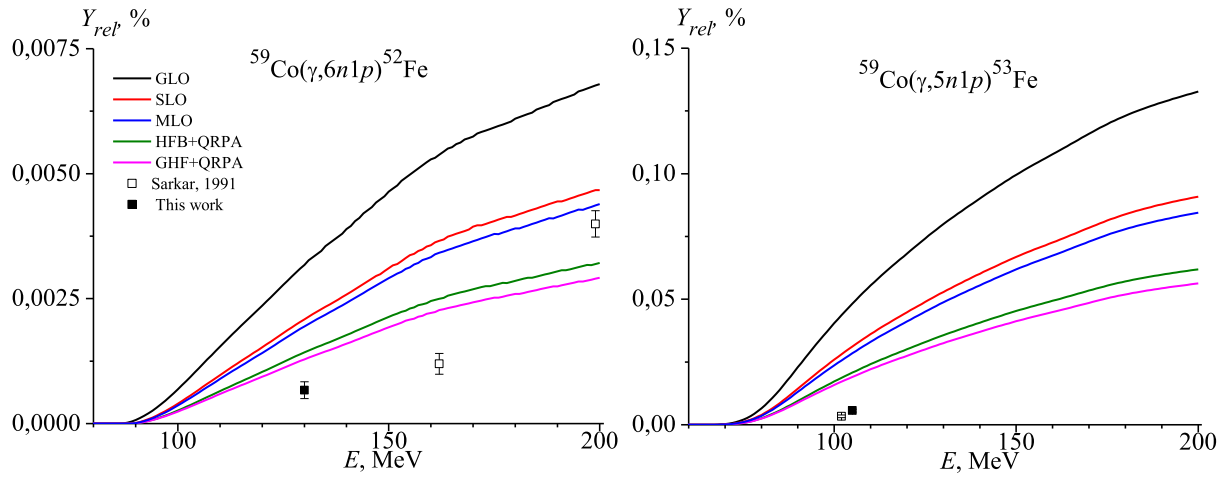

Fig. 5. (color online) Relative yields of the ^{59}Co(γ, xn1p)^{52,53}Fe reactions as a function of the bremsstrahlung end-point energy from the present work (solid squares) and literature data [4] (open triangles), [10] (open circles), and [13] (open squares), as well as the theoretically calculated values using different models for the $E1$ gamma-ray strength function in TALYS values.

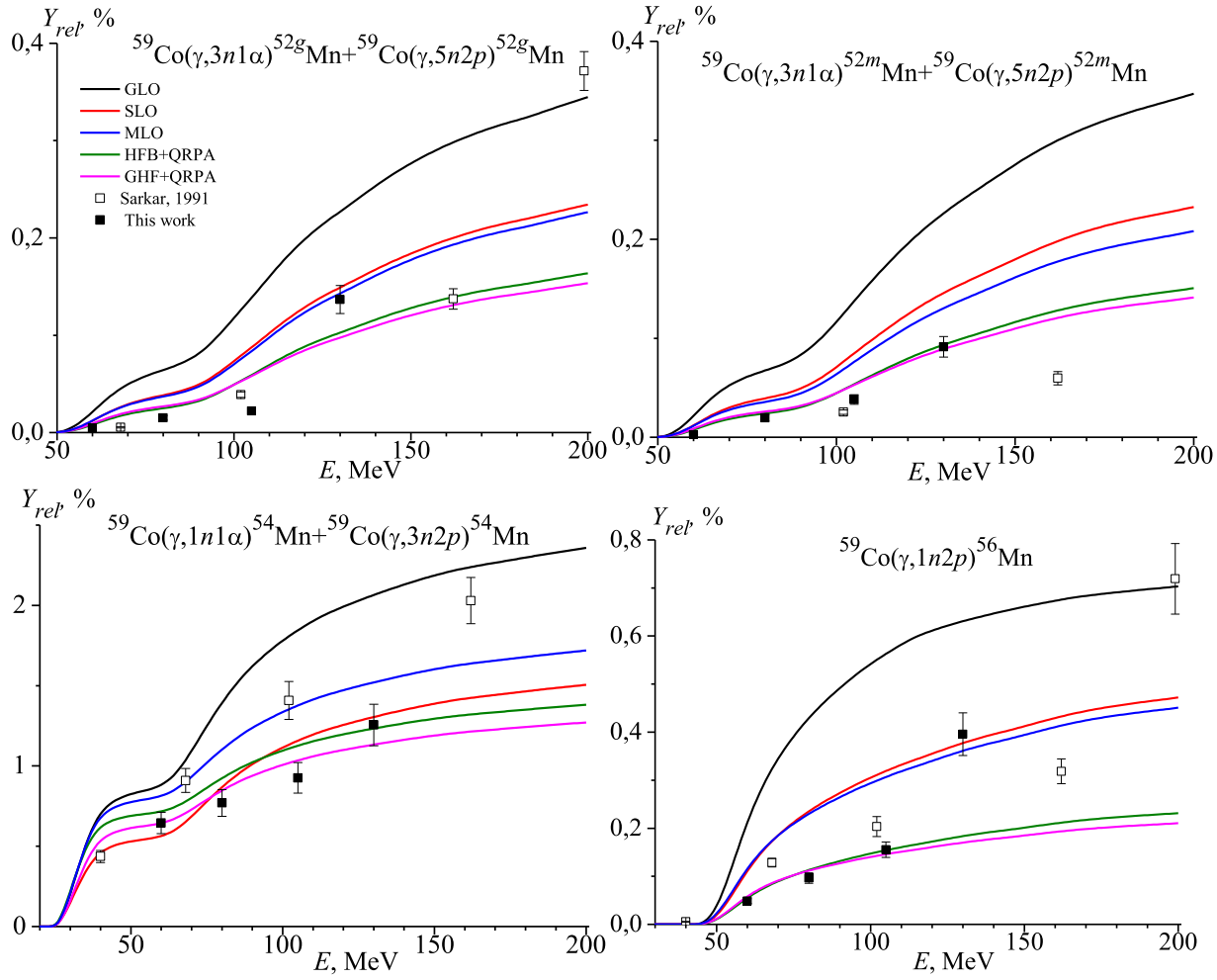

Fig. 6. (color online) Relative yields for the production of ^{52g,52m,54,56}Mn from reactions ^{59}Co(γ, x$n1\alpha$) and ^{59}Co(γ, x$n2p$) as a function of the bremsstrahlung end-point energy from the present study (solid squares), literature data [13] (open squares), and the theoretically calculated values using different models for the $E1$ gamma-ray strength function in TALYS values.

Figure 6 shows that the experimentally obtained relative yields for the production of ^{54}Mn at the bremsstrahlung end-point energy of 40 MeV are in agreement with the values simulated with TALYS, according to model GLO. Fig. 6 also shows that the relative yields for the production of ^{54}Mn are an order of magnitude greater than those for the reaction ^{59}Co(γ, $1n2p$)^{56}Mn.

Figure 6 shows that the experimentally obtained relative yields for the ^{59}Co(γ, $1n2p$)^{56}Mn reaction at the bremsstrahlung end-point energies of 40–100 MeV that are not in agreement with the values simulated with TALYS.

Finally, according to Fig. 6, it is clear that relative yields for reactions producing ^{54}Mn, ^{52g}Mn, and ^{52m}Mn are not constantly increasing functions. This is due to the fact that in the initial energy region, the main channels for the formation of the ^{54}Mn, ^{52g}Mn, and ^{52m}Mn isotopes are reactions with the emission of an alpha-particle. Near the energies of the reaction threshold, the ^{59}Co(γ, x$n2p$)^{54,52g,52m}Mn reaction is accompanied with the release of alpha-particles. Consequently, its cross sections decrease. A further increase in the relative yields is associated with the reactions ^{59}Co(γ, x$n2p$)^{54,52g,52m}Mn.

D. Reactions with the emission of three protons and several neutrons

It can be seen from Fig. 7 that the experimentally obtained relative yields for the production of ^{49}Cr at an energy of 102 MeV reported in previous studies [13] are not in agreement with the values simulated with TALYS based on different models. However, our experimental points are in agreement with the simulated values based on TALYS with models MLO and HFB+QRPA. Fig. 7 also shows that the experimentally obtained relative yields for the production of ^{51}Cr at energies of 102 and 162 MeV reported in the literature [13] are not in agreement with simulated values based on TALYS with different models.

Furthermore, Fig. 7 shows that the relative yields for

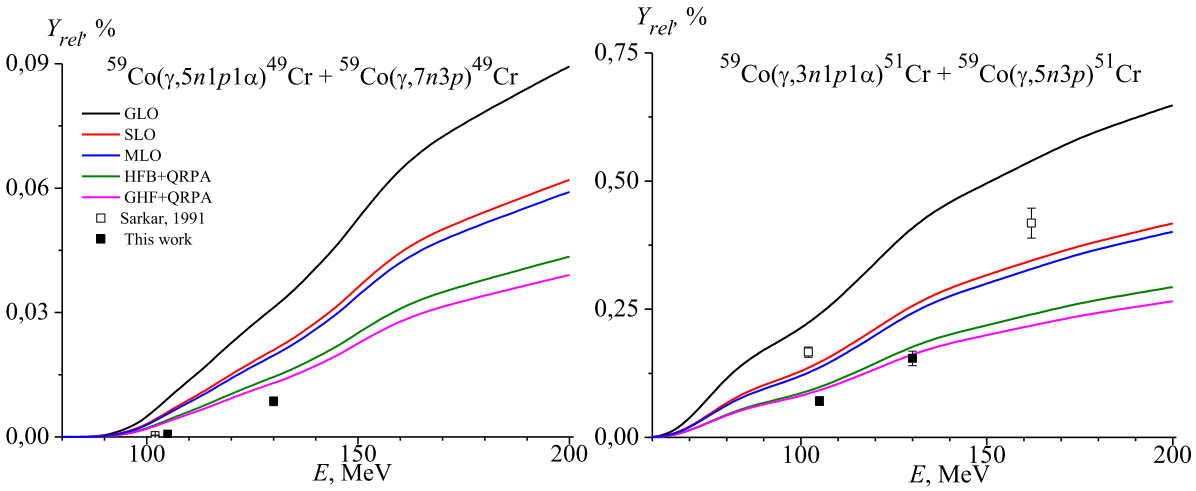

Fig. 7. (color online) Relative yields for the production of ^{49,51}Cr from reactions ^{59}Co(γ, x$n1p1\alpha$) and ^{59}Co(γ, x$n3p$) as a function of the bremsstrahlung end-point energy from the present study (solid squares), literature data [13] (open squares), as well as theoretically calculated values using different models for the $E1$ gamma-ray strength function in TALYS values.

reactions producing ^{51}Cr and ^{49}Cr are not constantly increasing functions. This is due to the fact that in the initial energy region, the main channels for the formation of ^{51}Cr and ^{49}Cr isotopes are reactions with emission of alpha-particles. At energies close to the threshold of the reactions ^{59}Co(γ, $5n3p$)^{51}Cr and ^{59}Co(γ, $7n3p$)^{49}Cr, the cross sections for reactions with the emission of alpha-particles decrease. Therefore, in this energy region in Fig. 7, a decrease in values was observed.

The $E1$ photon absorption by isotopes of the ^{59}Co (J^{π} = 7/2$^-$) nucleus leads to the excitation of the giant dipole resonance. Upon the decay of the giant dipole resonance via a reaction involving the emission of an alpha particle and three neutrons, a ^{52}Mn nucleus arises in the ground or excited state. Cascades of gamma transitions from excited states lead to the production of the isomeric or ground state of ^{52}Mn. The ^{52m}Mn isomeric state decays through electron capture or the isomer transition channel. The probability p for isomer transition to the ground state is 1.75%. Usually, the isomeric and ground states strongly differ in spins. Therefore, the isomeric ratio is represented in most cases through the yields of high- to low-spin states. In the case of ^{52m,g}Mn, the spin of the isomeric state of ^{52m}Mn is 2$^+$ (low-spin state, l) and that of the unstable ground state of ^{52g}Mn is 6$^+$ (high-spin state, h). Therefore, the isomeric ratio of ^{52m,g}Mn was computed as the ratio of the high- to low-spin states.

The isomeric ratios for the production of ^{52m,g}Mn from reactions ^{59}Co(γ, $3n1\alpha$) and ^{59}Co(γ, $5n2p$) at different bremsstrahlung end-point energies are plotted in Fig. 8.

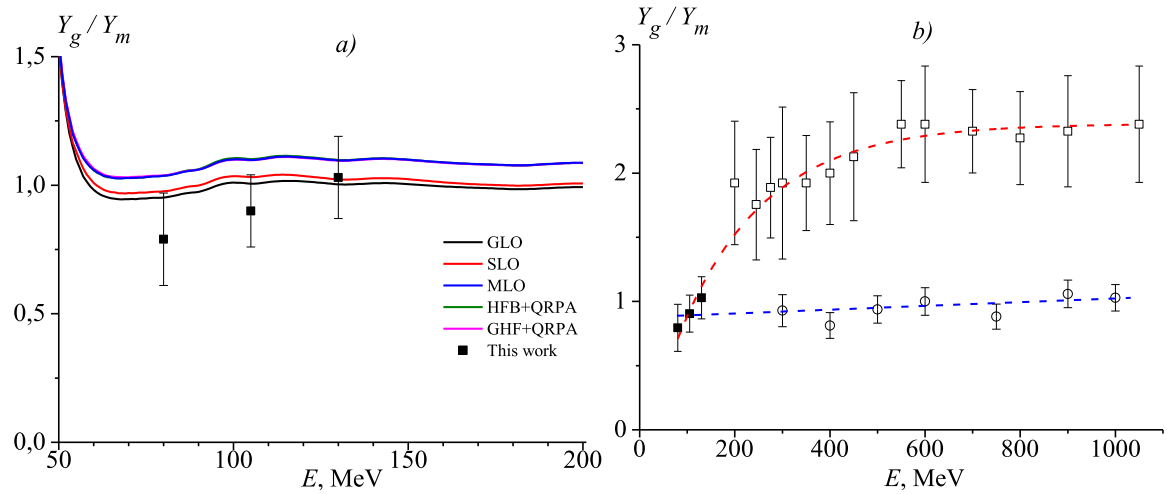

Fig. 8. (color online) Isomeric yield ratios of the pairs ^{52m,g}Mn produced in ^{59}Co(γ, $3n1\alpha$) and ^{59}Co(γ, $5n2p$) reactions as a function of the bremsstrahlung end-point energy from the present study (solid squares), literature data [10] (open circles), [13] (open squares), and the theoretically calculated values using different models for the $E1$ gamma-ray strength function in TALYS values.

The measured isomeric yield ratios for the pairs ^{52m,g}Mn at 80, 105, and 130 MeV are 0.79 ± 0.18, 0.90 ± 0.14, and 1.03 ± 0.16, respectively. Fig. 8(a) shows that the experimentally obtained isomeric ratio for the pairs ^{52m,g}Mn at the bremsstrahlung end-point energies of 80–130 MeV are in agreement with the values simulated with TALYS on the basis of GLO and SLO.Fig. 8(b) shows that our data on isomeric ratio complement the missing experimental data in the literature [10, 13]. Fig. 8(b) includes lines to guide the analysis of literature data [10] (blue dashed line) and [13] (red dashed line). The red line shows exponential growth in the region of 50−600 MeV and further saturation. The blue line coincides with an unchanged linear function surrounded by an isomer ratio value of 0.84. It is necessary to conduct experiments in the energy region of 130−300 MeV to obtain accurate information.

IV. CONCLUSIONS

Relative yields of the ^{59}Co(γ, xn; x = 1−4)$^{58\text{-}55}$Co, ^{59}Co(γ, 2pxn; x = 1−5)$^{56\text{-}52}$Mn, and ^{59}Co(γ, 3pxn; x = 5−7)^{51,49}Cr reactions at different bremsstrahlung end-point energies were obtained on the basis of the values simulated with TALYS. The data reported in this study along with those in the literature were found to be in good agreement with the simulated values. The relative yields for reactions producing ^{54,52g,52m}Mn and ^{49,51}Cr are not constantly increasing functions. This is due to the fact that in the initial energy region, the main channels for the formation of the ^{54,52g,52m}Mn and ^{49,51}Cr isotopes are reactions with the emission of an alpha-particle. Near the energies of the reaction threshold, the ^{59}Co(γ, xn2p)^{54,52g,52m}Mn and ^{59}Co(γ, xn3p)^{49,51}Cr reactions are accompanied by the release of alpha-particles; consequently, its cross sections decrease. The experimentally obtained isomeric ratio for the pairs ^{52m,g}Mn at the bremsstrahlung end-point energies of 80–130 MeV complement the missing experimental data in the literature.

ACKNOWLEDGMENT

The authors would like to thank the staff of the linear electron accelerator LINAC-200 (JINR) for their help with the described experiments.

References

[1] M. G. Davydov, F. Sh. Khamraev, and E. M. Shomurodov, At. Energ. **63**, 44 (1987)
[2] E. B. Bazhanov, A. P. Komar, and A. V. Kulikov, Eksp. Teor. Fiz. **46**, 1497 (1964)
[3] R. A. Alvarez, B. L. Berman, D. D. Faul *et al.*, Phys. Rev. C **20**, 128 (1979)
[4] S. C. Fultz, R. L. Bramblett, J. T. Caldwell *et al.*, Phys. Rev. **128**, 2345 (1962)
[5] G. Baciu, G. C. Bonazzola, B. Minetti *et al.*, Nucl. Phys. **67**, 178 (1965)
[6] R. Ghosh, B. Lawriniang, S. Badwar *et al.*, Radiochim. Acta. **106**, 345 (2018)
[7] G. Baciu, D. Catana, C. Deberth *et al.*, Nucl. Phys. A **167**, 177 (1971)
[8] A. G. Belov, Yu. P. Gangrskii, K. K. Gudima *et al.*, Atom. Ener. **88**, 408 (2000)
[9] B. I. Goryachev, B. S. Ishkhanov, I. M. Kapitonov *et al.*, Bull. Acad. Sci. **33**, 1588 (1969)
[10] H. Naik, G. Kim, M. Zaman *et al.*, Eur. Phys. J. A **55**, 217 (2019)
[11] H. Lichtblau and A. Goldmann, Z. Physik **205**, 47 (1967)
[12] A. N. Gorbunov, F. P. Denisov, and V. A. Kolotukhin, ZET **38**, 1084 (1960)
[13] S. R. Sarkar, M. Soto, Y. Kubota *et al.*, Radiochimica Acta **55**, 113 (1991)
[14] V. di Napoli, F. Salvetti, M. L. Terranova *et al.*, Journal of Inorganic and Nuclear Chemistry **40**, 175 (1978)
[15] A. Koning, S. Hilaire, and S. Goriely. TALYS-1.96: *A Nuclear Reaction Program*, User Manual, 2021 https://www-nds.iaea.org/talys/tutorials/talys_v1.96.pdf
[16] A. S. Dyatlov, *Inductive current sensor based on the rogowski coil*, in: *Bachelor Graduate Qualification Work* (Russia: University of Dubna, 2017) (in Russian) https://uni-dubna.ru/File?id=afdbddfd-b3ef-4aa0-b044-69d6892fd90d
[17] J. Frana, Journal of Radioanalytical and Nuclear Chemistry **257** (3), 583 (2003)
[18] Nudat 2.8, National Nuclear Data Center, Brookhaven National Laboratory, available from http://www.nndc.bnl.gov/nudat2/
[19] M. J. Berger and S. M. Seltzer, Phys. Rev. C **2**, 621 (1970)
[20] J. Kopecky and M. Uhl, Phys. Rev. C **41**, 1941 (1990)
[21] D. M. Brink, Nucl. Phys. **4**, 215 (1957)
[22] V. A. Plujko, O. M. Gorbachenko, R. Capote *et al.*, At. Data Nucl. Data Tables **123**, 1 (2018)
[23] S. Goriely and V. Plujko, Phys. Rev. C **99**, 014303 (2019)
[24] S. Goriely, E. Khan, and M. Samyn, Nucl. Phys. A **739**, 331 (2004)
[25] S. Goriely *et al.*, Phys. Rev. C **98**, 014327 (2018)
[26] J. Allison *et al.* , NIMA **835**, 186 (2016)